Desalination and Water Treatment
www.deswater.com

doi: 10.5004/dwt.2021.27304

227 (2021) 384–390
July

Adsorption of methylene blue onto Al-pillared montmorillonite

Chun-Yan Cao*, Min Wang*, Zhi-Guo Song, Shuang Zhao, Xin Wan

College of Chemistry and Materials Engineering, Bohai University, Jinzhou 121013, China,
emails: caochunyan_04@163.com (C.-Y. Cao), wangmin@bhu.edu.cn (M. Wang), lnbhu@hotmail.com (Z.-G. Song), shuangzhao_8123@126.com (S. Zhao), 9918648@qq.com (X. Wan)

Received 28 December 2020; Accepted 28 March 2021

ABSTRACT

Al-pillared montmorillonite (Al-MMT) was prepared with natural Na-type montmorillonite (Na-MMT) as raw material and aluminum polycation as a pillaring agent, which was evaluated as adsorbents for the removal of methylene blue (MB) from aqueous solutions. The materials were characterized by X-ray powder diffraction and N_2 adsorption–desorption at low temperatures. The results showed that the aluminum polycation was intercalated into the layer of MMT to form a stable aluminum oxide pillar after calcination, which resulted in an increase of surface area and layers spacing of MMT. The adsorption capacity of Al-MMT for MB was higher than that of Na-MMT. Freundlich isotherm and pseudo-second-order kinetic models were more suitable to describe the adsorption process of MB on Al-MMT. The thermodynamic parameters indicated that the adsorption process was endothermic and spontaneous. The increasing solution pH could lead to an increase in the adsorption capacity of Al-MMT for MB.

Keywords: Al-pillared montmorillonite; Methylene blue; Dyestuff pollutants; Adsorption

1. Introduction

With the rapid development of the textile, printing and dyeing industry, the discharge of dyestuff wastewater has been a noticeable increase. Furthermore, dyestuff wastewater has the characteristic of strong toxicity, difficulty biochemical degradation, and stability to light, heat and oxidizing agents, which seriously threatens the ecological environment and human health [1–4]. Methylene blue (MB) is a cationic dye with a heterocyclic aromatic compound containing sulfur. It is toxic and can cause serotonin syndrome, hypertension, skin staining, hemolytic anemia, injection site necrosis and precordial pain [5,6]. Therefore, the treatment of MB wastewater has attracted the great attention of researchers.

Numerous approaches have been developed to treat dyestuff wastewater, including chemical oxidation, membrane separation, flocculation-coagulation, adsorption, aerobic or anaerobic treatment, and so on [1,7–9]. Among these methods, adsorption is an effective method used for dye removal due to its advantages of simple operation, low cost and high efficiency [1,9]. Several porous materials such as activated carbon, zeolites, metal-organic frameworks, nanoparticle and polymer-based materials were used as adsorbents for treatment dyestuff wastewater and exhibited higher adsorption efficiency [6,10–14]. Compared with these materials, various industrial and agricultural waste materials (e.g., hen feather, eggshell, fly ash, etc.) [15–17] and natural clay minerals (e.g., bentonite, diatomite, illite, halloysite, etc.) [18–21] used as adsorbent have enhanced the usefulness of the adsorption process for the removal of various dye due to low-cost, environmentally friendly and easy to obtain.

The use of clay minerals, especially montmorillonite (MMT), as adsorbents has attracted more and more attention due to their abundant resources, cheaper, thermal and chemical stability in a wide range of pH, high cation

* Corresponding authors.

exchange capacity and surface area [22]. MMT, a 2:1-layered aluminosilicate, is composed of an Al octahedral sheet situated between two Si tetrahedral sheets. In the mineral lattice, the partial isomorphous substitution of Al^{3+} with Fe^{2+} and Mg^{2+} in the octahedral positions and Si^{4+} with Al^{3+} in the tetrahedral positions make the layers negatively charged, which is balanced by the exchangeable cations (such as Na^{+}, Ca^{2+}) in the interlayer space [23,24]. However, the adsorption capacity of MMT for organic dye may be limited by their small basal spaces [25]. To enhance the adsorption capacity of MMT for dye, the interlayer spaces of MMT had been expanded by intercalation with large organic molecules (such as quaternary ammonium compound cation surfactant, cetyltrimethylammonium bromide). Although the organic intercalated clays exhibited high adsorption capacity for dye, organic molecules were not resistant to high temperatures (higher than 250°C) [26], which made regeneration of used organic intercalated clays difficult. In addition, pillared interlayered clays (PILCs) prepared by using inorganic metal polyhydroxy cations to replace the original cations in the clay minerals had high surface areas, large interlayer spaces, thermal stabilities, and it also presented high adsorption capacity for dye [1,25,27]. Furthermore, it was easy to achieve regeneration for PILCs absorbed dye via heating. The properties of PILCs could be modified and optimized to suit a specific application by using different pillaring agents and synthetic conditions including concentration of metal ions, pH, aging time, temperature and metal/clay ratio, which influenced the adsorption behavior of organic dye.

Based on these understandings, the objective of this work was to prepare Al-pillared montmorillonite (Al-MMT) and explore its application as adsorbents for the removal of MB from an aqueous solution. Several adsorption parameters such as contact time, temperature, pH, and the initial MB concentration were investigated in detail. Meanwhile, the adsorption kinetics and isotherms for MB on the Al-MMT were determined.

2. Materials and methods

2.1. Materials

Purified Na-type montmorillonite (Na-MMT) was purchased from Zhejiang Sanding Group Co., Ltd., China, and the cation exchange capacity (CEC) of which is 110 mmol/100 g. MB solutions of known concentrations were prepared by dissolving a certain amount of MB (analytical reagent grade) in deionized water.

2.2. Sample preparation

The alumina pillaring solution was prepared by using $AlCl_3$ as the pillar precursor, that is, Na_2CO_3 aqueous solution (0.25 mol L^{-1}) was slowly added to $AlCl_3$ aqueous solution (0.25 mol L^{-1}) under vigorous stirring at 60°C until an OH^{-}/Al^{3+} molar ratio of 2.2 was reached. Then, the mixture was aged at 60°C for 24 h and obtaining the alumina polycation solution.

Subsequently, the mixture was added dropwise into a 2 wt.% suspension of Na-MMT, keeping the Al^{3+}/Na-MMT ratio of 2 CEC. The final suspension was stirred at 60°C for 12 h and aged for the additional 12 h at the same temperature. Then, the suspension was centrifuged, washed with deionized water until no chloride was detected, and dried at 80°C. Subsequently, the sample was heated at 500°C for 4 h at a ramping rate of 2°C min^{-1}. The alumina pillared MMT was obtained and abbreviated as Al-MMT.

2.3. Characterization of sample

X-ray powder diffraction (XRD) patterns were obtained by a Bruker D8 ADVANCE X-ray diffractometer using monochromatized Cu/Kα radiation (40 kV, 40 mA). The samples were scanned with a step size of 0.02° and a counting time of 0.2 s per step. The N_2 adsorption–desorption isotherms of samples were recorded at –196°C using BelSorp-Max (BEL Japan Inc.). Prior to analysis, the samples (ca. 1,000 mg) were outgassed at 350°C for 5 h. The surface areas were calculated using the Brunauer–Emmett–Teller equation.

2.4. Batch adsorption experiments

Batch adsorption experiments were carried out in a group of 250 mL stoppered conical flasks with 100 mL MB solution, and the pH was adjusted using dilute HCl or NaOH solutions. Subsequently, a certain amount of Al-MMT was added. The mixture was then agitated on a constant temperature oscillator. After centrifuging, the supernatant was then analyzed for residual concentration of MB using a spectrophotometer.

3. Results and discussion

3.1. Characteristics of samples

The XRD patterns of the Na-MMT and Al-MMT are shown in Fig. 1. The changes of the layered structure of MMT pillared by alumina were clearly observed from the characteristic (001) diffraction. The (001) diffraction peak of Na-MMT was at 2θ of about 9.2°, indicating the basal

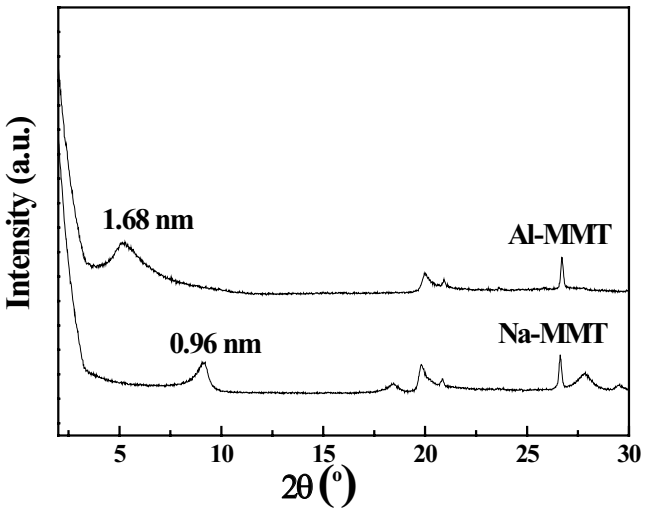

Fig. 1. XRD patterns for Na-MMT and Al-MMT.

spacing of 0.96 nm as calculated by Bragg's equation. The d001 spacing of the Al-MMT was 1.68 nm according to its diffraction peak at 4.75°. The increase of the d001 spacing could be ascribed to the aluminum polycation intercalated into the layer of MMT to form a stable aluminum oxide pillar after calcination. Moreover, the (001) diffraction peak of Al-MMT was slightly broader compared to that of Na-MMT. This manifested the crystallinity of MMT decreased and the layer structure wasn't destroyed after the intercalating aluminum polycation into Na-MMT.

As demonstrated in Fig. 2, N_2 adsorption–desorption isotherms of Al-MMT were distinctly different from that of Na-MMT. The volume of N_2 adsorbed by Al-MMT increased obviously in the range of $p/p_0 < 0.1$, which indicated that a large number of micropores were created after Na-MMT pillared by alumina. Based on the IUPAC classification [28], Al-MMT showed a type IV isotherm with an H4-type hysteresis loop that appeared above a relative pressure of 0.45, indicating the slit-shaped open-pore mesopores structure were created after Na-MMT pillared by alumina [29].

Taking into account the specific surface area (Table 1), Na-MMT was only 28 $m^2\ g^{-1}$, and Al-MMT displayed a higher specific surface area (196 $m^2\ g^{-1}$). The increase of specific surface area demonstrated the incorporation of pillars between the layers of Na-MMT resulting in a well-defined porous framework, which was confirmed by pore size. The average pore size of Al-MMT (2.9 nm) induced by the formation of aluminum oxide pillar in the interlayer of MMT was obviously low than that of Na-MMT (15.3 nm), which was supported by XRD results.

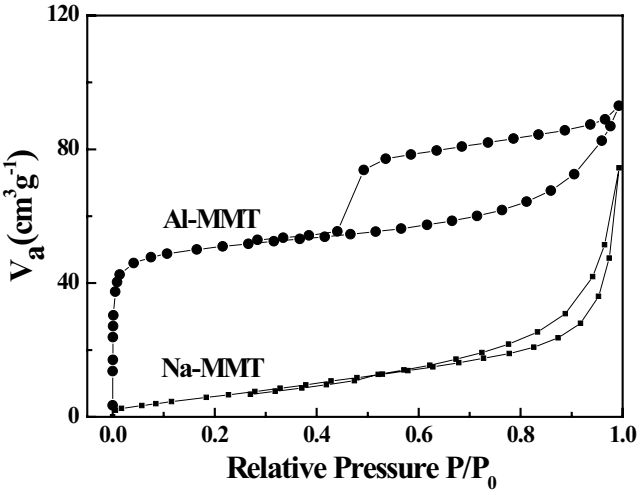

Fig. 2. N_2 adsorption–desorption isotherms of Na-MMT and Al-MMT.

3.2. MB adsorption

3.2.1. Effect of adsorbent type

The adsorption capacity of MB on Na-MMT and Al-MMT under the condition of initial MB concentration of 50 mg L^{-1}, the solution pH of 6, the adsorbent dosage of 0.3 g L^{-1}, and contact time of 60 min was listed in Table 1. In comparison to Na-MMT, Al-MMT exhibited higher adsorption capacity. It is commonly accepted that the larger the surface area of adsorbents, the higher the adsorption capacity. Thus, Al-MMT with a larger specific surface area showed a higher adsorption capacity under the same adsorption condition. In addition, when the pore size of the adsorbent was 1.3–1.8 times the diameter of the solute molecule, the adsorption of solute molecules would easily take place [30]. Therefore, based on the MB dimensions (1.43 nm × 0.61 nm × 0.4 nm) and considering that the MB molecules most likely diffused lengthwise into the porous structure of the adsorbent [31], and assuming that the adsorbent pore size was 1.8 times the MB molecular diameter, this implied a minimum adsorbent pore size of 1.10 nm for MB. Consequently, the MB diffusion into the pores of Al-MMT (basal spacing of 1.68 nm) was easier than that of Na-MMT (basal spacing of 0.96 nm) and then resulting in the increasing adsorption capacity of MB on Al-MMT. This result suggested that MMT with a large specific surface area and interlayer spacing favored MB adsorption. These findings demonstrated that the pore structure of the adsorbents had an important influence on the adsorption capacity of dyes.

3.2.2. Effect of contact time and adsorption kinetics

The adsorption data of MB on Al-MMT vs. contact time is illustrated in Fig. 3. The adsorption capacity of Al-MMT for MB increased rapidly in the first 40 min, which indicated the adsorption rate was very fast. With further increasing the contact time, the adsorption of MB increased slowly. In the initial adsorption period, a large number of adsorption sites were available for adsorption of MB. Furthermore, the MB concentration difference between the bulk solution and the solid-liquid interface, that is, the driving force of adsorption, was higher. Therefore, these led to rapid adsorption. However, further increasing the time, the number of available surface sites decreased with a filling of MB molecules, and the driving force of adsorption would be decreased due to decreasing MB concentration in bulk solution. Thus, it resulted in a decrease in the adsorption rate.

In order to clarify the potential rate-controlling steps involved in the process of adsorption of MB on Al-MMT, two

Table 1
Summary of the textural properties and adsorption capacity of different MMTs

Samples	Brunauer–Emmett–Teller surface area ($m^2\ g^{-1}$)	Pore volume ($cm^3\ g^{-1}$)	Average pore size (nm)	Adsorption capacity ($mg\ g^{-1}$)
Na-MMT	28	0.11	15.3	58.53
Al-MMT	196	0.14	2.9	86.79

conventional kinetic models (pseudo-first-order Eq. (1) and pseudo-second-order model Eq. (2)) were applied to describe the adsorption in solid–liquid systems.

$$\text{Pseudo-first-order: } q_t = q_e\left(1 - e^{-k_1 t}\right) \quad (1)$$

$$\text{Pseudo-second-order: } q_t = \frac{q_e^2 k_2 t}{1 + q_e k_2 t} \quad (2)$$

where q_e and q_t are the amount of MB adsorbed (mg g^{-1}) at equilibrium and any time t (min), respectively; k_1 and k_2 are the pseudo-first-order model rate constant (min^{-1}), and the pseudo-second-order kinetics model rate constant (g mg^{-1} min^{-1}), respectively.

The kinetics parameters for the adsorption of MB on Al-MMT were calculated via non-linear fitting analysis of the experiment data (Fig. 3) using pseudo-first-order and pseudo-second-order kinetic models, that is, the q_e (96.03) and k_1 (0.055) of pseudo-first-order kinetics, the q_e (114.06) and k_2 (0.000537) of pseudo-second-order kinetics. The correlation coefficient (R^2) of the pseudo-second-order kinetics model (0.9923) was greater than that of the pseudo-first-order kinetics model (0.9678) for the adsorption of MB on Al-MMT. Therefore, the pseudo-second-order kinetics model was more suitable to describe the adsorption process of MB on Al-MMT. This demonstrated that chemisorption, rather than diffusion/ion exchange, was the rate-limiting step to adsorption [32,33]. Furthermore, it could be found that the equilibrium adsorption capacity calculated by pseudo-second-order kinetics was closer to the experimental value, which further confirmed that the adsorption process would meet pseudo-second-order kinetics.

3.2.3. Impact of MB concentration and adsorption isotherms

The effects of initial MB concentration on the adsorption performance of Al-MMT are presented in Fig. 4. The amounts of MB adsorbed on the Al-MMT increased with increasing initial MB concentration. At low MB concentration, the ratio of the MB molecules to the available adsorption sites of Al-MMT was low and consequently, the adsorption was independent of the Al-MMT. However, with increasing the number of MB molecules, the unit mass of the Al-MMT exposing to more MB molecules, and the Al-MMT with more available adsorption sites would take up more MB molecules. Moreover, with the increase of MB concentration in the aqueous phase, the increasing difference of concentration between the solid-liquid phase would enhance the interaction of MB with the Al-MMT. Therefore, the amounts of MB absorbed by Al-MMT increased with increasing initial MB concentration. In addition, it can be seen from Fig. 4, the absorption capacity (q_e) increased quickly at low initial MB concentration, while the increase of q_e was slowed down at higher initial MB concentration due to decreasing the adsorption sites in the Al-MMT.

In order to elaborate the interaction between the adsorbate and adsorbent, the experimental equilibrium MB adsorption data (q_e) at various residual MB concentrations (C_e) was fitted by Langmuir, Freundlich, Temkin, and Dubinin-Radushkevich (D-R) isotherm models, as shown in Eqs. (3)–(6) [34]. The fitting curves of these isothermal models are presented in Fig. 5.

$$\text{Langmuir isotherm: } q_e = \frac{q_{\max} K_L C_e}{1 + K_L C_e} \quad (3)$$

$$\text{Freundlich isotherm: } q_e = K_F C_e^{1/n} \quad (4)$$

$$\text{Temkin isotherm: } q_e = \frac{RT}{b_T}\ln\left(A_T C_e\right) \quad (5)$$

$$\text{D-R isotherm: } q_e = q_m e^{-K_D\left[RT\ln\left(1+1/C_e\right)\right]^2} \quad (6)$$

where C_e (mg L^{-1}) and q_e (mg g^{-1}) are the MB concentration in the solution and the amount of adsorbed MB on the Al-MMT at equilibrium, respectively; $q_{\max}$ (mg g^{-1}) and K_L

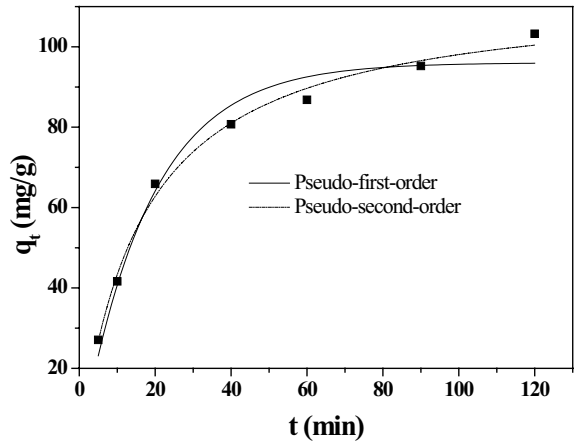

Fig. 3. The fit of adsorption kinetics of MB onto Al-MMT. Experimental condition: adsorbent dose 0.3 g L^{-1}; initial pH 6; MB concentration 50 mg L^{-1}; adsorption temperature 35°C.

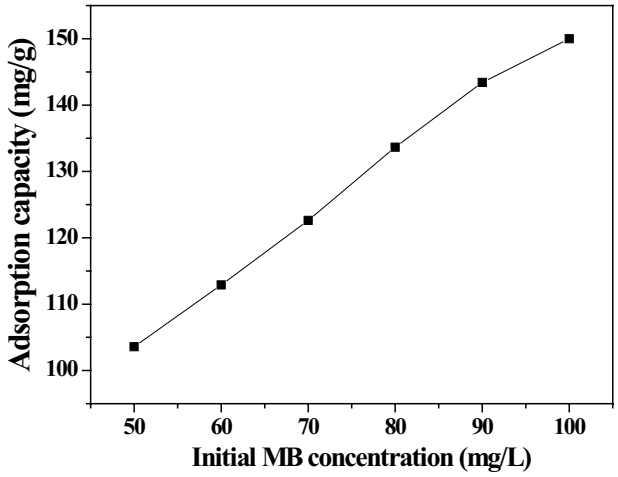

Fig. 4. Effect of initial MB concentration on the adsorption capacity. Experimental condition: adsorbent dose 0.3 g L^{-1}; initial pH 6; contact time 120 min; adsorption temperature 35°C.

(L mg^{-1}) are the Langmuir isotherm constants, that is, the maximum adsorption capacity and the energy of adsorption, respectively; K_F and n are the Freundlich isotherm parameters related to adsorption capacity and intensity of adsorption, respectively; b_T and A_T are the Temkin isotherm constant related to the heat of adsorption and the equilibrium binding constant corresponding to the maximum binding energy, respectively; q_m (mg g^{-1}) and K_D (mol^2 kJ^{-2}) are the D-R isotherm parameters related the maximum adsorption capacity and adsorption parameter strength, respectively. R (J mol^{-1} K^{-1}) is the gas constant, T (K) denotes the temperature.

The isothermal adsorption parameters for the adsorption of MB was estimated via non-linear fitting analysis of the experiment data (Fig. 5), that is, q_{max} (199.2) and K_L (0.0525) of Langmuir isotherm, K_F (34.6) and $1/n$ (0.366) of Freundlich isotherm, b_T (56.75) and A_T (0.4901) of Temkin isotherm, q_m (150.7) and K_D (25.168) of D-R isotherm. According to the correlation coefficients (R^2) of the non-linearized form of isotherm models, that is, Langmuir (0.9624), Freundlich (0.9892), Temkin (0.9762), and D-R (0.8360), it could be considered that the adsorption process of MB on Al-MMT could be described by the Langmuir, Freundlich and Temkin isotherm models, however, Freundlich isotherm model was more adapted to describe the adsorption process of MB on Al-MMT due to the R^2 of Freundlich isotherm models higher than that of others, which indicated that the adsorption of MB on Al-MMT belongs to multilayer adsorption.

In addition, based on the $1/n$ value of the Freundlich isotherm, the adsorption process could be classified as irreversible ($1/n = 0$), favorable ($0 < 1/n < 1$), or unfavorable ($1/n > 1$) [35,36]. In this work, the parameter $1/n$ was 0.366, which demonstrated a favorable adsorption took place at a heterogeneous surface of Al-MMT.

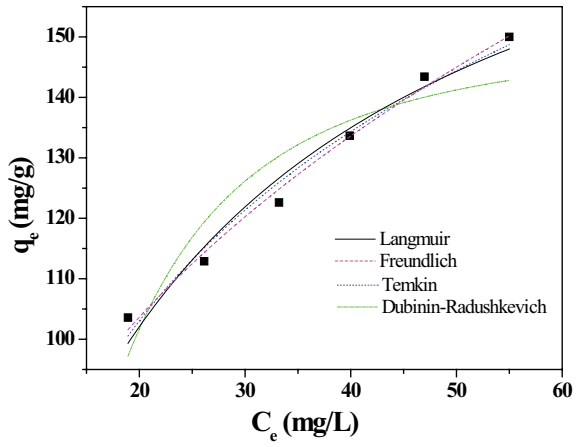

Fig. 5. Adsorption isotherms fit of MB onto Al-MMT. Experimental condition: adsorbent dose 0.3 g L^{-1}; initial pH 6; contact time 120 min; adsorption temperature 35°C.

3.2.4. Impact of adsorption temperature and adsorption thermodynamic

The effect of adsorption temperature on the adsorption performance of Al-MMT was performed by varying the temperature under the condition of adsorbent dose 0.3 g L^{-1}, initial pH 6, MB concentration 50 mg L^{-1}, and contact time 60 min, and the adsorption capacity of Al-MMT at 25°C, 35°C and 45°C were 53.56, 86.79 and 110.71 mg g^{-1}, respectively. The diffusion rate of molecules in high temperature would be rapid and a large number of molecules to acquire enough energy to engage an interaction with active sites on the surface of adsorbent [37]. Therefore, the adsorption capacity of Al-MMT was increased with increasing of adsorption temperature.

The thermodynamic analysis for MB adsorption on Al-MMT was implemented in order to explore whether the adsorption process of MB on Al-MMT was endothermic or exothermic, spontaneous or nonspontaneous. The free energy change (ΔG), enthalpy change (ΔH) and entropy change (ΔS) could be estimated by Eqs. (7) and (8).

$$\Delta G = -RT\ln k_d \tag{7}$$

$$\Delta G = \Delta H - T\Delta S \tag{8}$$

where R, T, k_d are the universal gas constant (8.314 J mol^{-1} K^{-1}), the temperature in Kelvin, and the distribution coefficient, respectively. Based on Eqs. (7) and (8), a linear form Eq. (9) would be gained.

$$\ln k_d = \frac{-\Delta H}{RT} + \frac{\Delta S}{R} \tag{9}$$

ΔS and ΔH could be obtained from Eq. (9).

According to Eq. (7) and $k_d = q_e/C_e$, the values of ΔG and k_d were calculated at 25°C, 35°C, and 45°C, and the results are shown in Table 2. The values of ΔH and ΔS gained from slope and intercept of linear plots of $\ln k_d$ vs. $1/T$ are presented in Table 2.

It is common knowledge that the negative ΔG suggests the forward reaction is spontaneous, and the positive ΔG suggests the backward reaction is spontaneous, while $\Delta G = 0$ demonstrates the system has reached an equilibrium state. For MB adsorption on Al-MMT, ΔG was negative at different adsorption temperatures, which manifested that the adsorption of MB on the Al-MMT was a spontaneous process. And the absolute value of ΔG raised with the increase of adsorption temperature, which indicated that

Table 2
Parameters of thermodynamics for MB adsorption by Al-MMT

k_d			ΔG (kJ mol^{-1})			ΔH (kJ mol^{-1})	ΔS (J mol^{-1} K^{-1})
25°C	35°C	45°C	25°C	35°C	45°C		
1.5785	3.6219	6.5954	–1.13	–3.30	–4.99	56.46	193.41

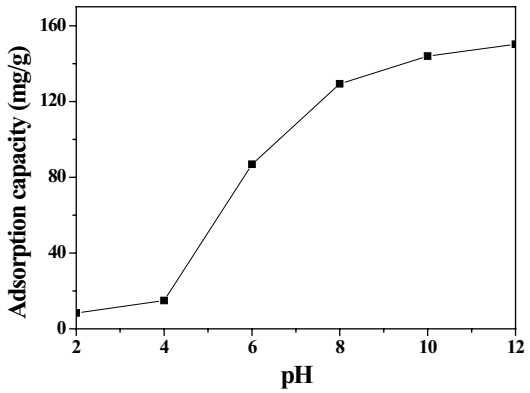

Fig. 6. Effect of initial pH on MB adsorption onto Al-MMT. Experimental condition: adsorbent dose 0.3 g L^{-1}; MB concentration 50 mg L^{-1}; contact time 60 min; adsorption temperature 35°C.

increasing temperature could increase the spontaneity of adsorption. The ΔH value was positive, which suggested that the adsorption process was endothermic, thus an appropriate increase in the adsorption temperature was beneficial to the adsorption. This was proved by the experimental data. Furthermore, the value of ΔH could confirm whether adsorption was the physical adsorption or chemisorption. Generally, in the case of absolute physical adsorption, the ΔH value was less than 20 kJ mol^{-1}, and if ΔH value was in the range of 80–200 kJ mol^{-1}, it was chemisorption [38,39]. In this work, the value of ΔH was 56.46 kJ mol^{-1}, suggesting that MB adsorption processes would be considered as between physical adsorption and chemisorption. The ΔS value was positive, which manifested that the adsorption of MB on solid–liquid interface of Al-MMT was disordered and accompanied with greater confusion.

3.2.5. *Effect of initial pH on adsorption*

The influence of initial pH on the adsorption of MB on Al-MMT is shown in Fig. 6. The adsorption capacity increased with increasing pH. Generally, the surface charge of the adsorbent was affected by pH of solution due to protonation and deprotonation phenomenon [40–42]. When pH was lower, the surface of adsorbent would be positively charged because of protonation. The repulsive forces which existed between the positive MB molecules and the surface of the adsorbent would result in poor adsorption of MB. Whereas, when the pH was higher, it would generate more negatively charged active sites at the adsorbent surface due to deprotonate, and then leading to the higher uptake of cationic MB. In addition, at low pH, H^+ ions would compete with cationic MB molecule, and then resulting in lower adsorption capacity of Al-MMT. The inhibitory effect of H^+ ions on the adsorption of MB would decrease with increasing pH [43,44], this was another reason why the adsorption capacity of Al-MMT increased with increasing pH of solution.

4. Conclusion

Na-MMT was pillared with aluminum polycation to prepare Al-MMT with high specific surface and pore volume due to forming many micro-mesopores induced by introduction of aluminum into MMT. The Al-MMT showed a higher adsorption capacity of MB than Na-MMT. The adsorption kinetics and adsorption isotherm of MB on Al-MMT conformed to the pseudo-second-order kinetics model and Freundlich model, respectively. The MB adsorption process on the Al-MMT was demonstrated to be an endothermic and spontaneous process. The increase of solution pH resulted in increasing of adsorption capacity due to the decreased inhibitory effect of H^+ ions on the adsorption of MB and increasing of negatively charged active sites at the surface of adsorbent.

Acknowledgments

This work was supported by the National Natural Science Foundation of China (No. 21707009), Institute of Ocean Research, Bohai University (No. 05019/XK202030-3), the Doctor Startup Research Foundation of Bohai University (No. 0159bs009). Natural Science Foundation of Liaoning Province (No. 2019-MS-005), the Education Department Project of Liaoning Province (No. LJ2019007), the Doctor Startup Research Foundation of Liaoning Province (No. 2019-BS-005).

References

[1] Y.-F. Hao, L.-G. Yan, H.-Q. Yu, K. Yang, S.-J. Yu, R.-R. Shan, B. Du, Comparative study on adsorption of basic and acid dyes by hydroxy-aluminum pillared bentonite, J. Mol. Liq., 199 (2014) 202–207.
[2] G. Kyzas, N.K. Lazaridis, A.C. Mitropoulos, Removal of dyes from aqueous solutions with untreated coffee residues as potential low-cost adsorbents: equilibrium, reuse and thermodynamic approach, Chem. Eng. J., 189–190 (2012) 148–159.
[3] J. Ma, B. Cui, J. Dai, Mechanism of adsorption of anionic dye from aqueous solutions onto organobentonite, J. Hazard. Mater., 186 (2011) 1758–1765.
[4] J. Mittal, Permissible synthetic food dyes in India, Resonance, 25 (2020) 567–577.
[5] B.S. Kaith, J. Sharma, Sukriti, S. Sethi, T. Kaur, U. Shankar, V. Jassal, Fabrication of green device for efficient capture of toxic methylene blue from industrial effluent based on $K_2Zn_3[Fe(CN)_6]_2{\cdot}9H_2O$ nanoparticles reinforced gum xanthan-psyllium hydrogel nanocomposite, J. Chin. Adv. Mater. Soc., 4 (2016) 249–268.
[6] C. Arora, S. Soni, S. Sahu, J. Mittal, P. Kumar, P.K. Bajpai, Iron based metal organic framework for efficient removal of methylene blue dye from industrial waste, J. Mol. Liq., 284 (2019) 343–352.
[7] E. Altintig, M. Daglar, H. Altundag, Removal of methylene blue with nanomagnetic coated wild chestnut shells: thermodynamic, kinetic, isotherm, and mechanism studies, Desal. Water Treat., 207 (2020) 398–409.
[8] M.T. Yagub, T.K. Sen, S. Afroze, H.M. Ang, Dye and its removal from aqueous solution by adsorption: a review, Adv. Colloid Interface Sci., 209 (2014) 172–184.
[9] J.E. Aguiar, J.A. Cecilia, P.A.S. Tavares, D.C.S. Azevedo, E. Rodríguez Castellón, S.M.P. Lucena, I.J. Silva Junior, Adsorption study of reactive dyes onto porous clay heterostructures, Appl. Clay Sci., 135 (2017) 35–44.
[10] H. Daraei, A. Mittal, Investigation of adsorption performance of activated carbon prepared from waste tire for the removal of methylene blue dye from wastewater, Desal. Water Treat., 90 (2017) 294–298.
[11] N. Mirzaei, A.H. Mahvi, H. Hossini, Equilibrium and kinetics studies of direct blue 71 adsorption from aqueous solutions using modified zeolite, Adsorpt. Sci. Technol., 36 (2018) 80–94.

[12] S. Soni, P.K. Bajpai, D. Bharti, J. Mittal, C. Arora, Removal of crystal violet from aqueous solution using iron based metal organic framework, Desal. Water Treat., 205 (2020) 386–399.
[13] I. Anastopoulos, A. Hosseini-Bandegharaei, J. Fu, A.C. Mitropoulos, G.Z. Kyzas, Use of nanoparticles to dye adsorption: a review, J. Dispersion Sci. Technol., 39 (2017) 836–847.
[14] S. Soni, P.K. Bajpai, J. Mittal, C. Aror, Utilisation of cobalt doped iron based MOF for enhanced removal and recovery of methylene blue dye from waste water, J. Mol. Liq., 314 (2020) 113642, doi: 10.1016/j.molliq.2020.113642.
[15] J. Mittal, V. Thakur, A. Mittal, Batch removal of hazardous azo dye Bismark Brown R using waste material hen feather, Ecol. Eng., 60 (2013) 249–253.
[16] M.A. Abdel-Khalek, M.K.A. Rahman, A.A. Francis, Exploring the adsorption behavior of cationic and anionic dyes on industrial waste shells of egg, J. Environ. Chem. Eng., 5 (2017) 319–327.
[17] D.S. Sun, X.D. Zhang, Y.D. Wu, X. Liu, Adsorption of anionic dyes from aqueous solution on fly ash, J. Hazard. Mater., 181 (2010) 335–342.
[18] F. Gomri, M. Boutahala, H. Zaghouane-Boudiaf, S.A. Korili, A. Gil, Removal of acid blue 80 from aqueous solutions by adsorption on chemical modified bentonites, Desal. Water Treat., 57 (2016) 1–10.
[19] Y.-H. Zhao, J.-T. Geng, J.-C. Cai, Y.-F. Cai, C.-Y. Cao, Adsorption performance of basic fuchsin on alkali-activated diatomite, Adsorpt. Sci. Technol., 38 (2020) 151–167.
[20] B.A. Fil, M. Korkmaz, C. Özmetin, Application of nonlinear regression analysis for methyl violet (MV) dye adsorption from solutions onto illite clay, J. Dispersion Sci. Technol., 37 (2016) 991–1001.
[21] I. Anastopoulos, A. Mittal, M. Usman, J. Mittal, G. Yu, A. Núñez-Delgado, M. Kornaros, A review on halloysite-based adsorbents to remove pollutants in water and wastewater, J. Mol. Liq., 269 (2018) 855–868.
[22] V.K. Gupta, Application of low-cost adsorbents for dye removal – a review, J. Environ. Manage., 90 (2009) 2313–2342.
[23] G.D. Yuan, B.K.G. Theng, G.J. Churchman, W.P. Gates, Clays and Clay Minerals for Pollution Control, F. Bergaya, B.K.G. Theng, G. Lagaly, Eds., Handbook of Clay Science, Elsevier, Amsterdam, Netherlands, 2006, pp. 625–675.
[24] Y.-H. Zhao, F. Ma, K. Tang, Preparation of acid-activated montmorillonite and its application, Mar. Georesour. Geotechnol., 34 (2016) 741–746.
[25] P. Tepmatee, P. Siriphannon, Effect of preparation method on structure and adsorption capacity of aluminum pillared montmorillonite, Mater. Res. Bull., 48 (2013) 4856–4866.
[26] F. Bergaya, A. Aouad, T. Mandalia, Pillared Clays and Clay Minerals, F. Bergaya, B.K.G. Theng, G. Lagaly, Eds., Handbook of Clay Science, Elsevier, Amsterdam, Netherlands, 2006, pp. 393–421.
[27] Z. Bouberka, A. Khenifi, N. Benderdouche, Z. Derriche, Removal of supranol yellow 4GL by adsorption onto Cr-intercalated montmorillonite, J. Hazard. Mater., 133 (2006) 154–161.
[28] K.S.W. Sing, D.H. Everett, R.A.W. Haul, L. Moscou, R.A. Pierotti, J. Rouquerol, T. Siemieniewska, Reporting physisorption data for gas/solid systems with special reference to the determination of surface area and porosity, Pure Appl. Chem., 57 (1985) 603–619.
[29] J.K.P. Jong, J. Zecevic, H. Friedrich, P.E. Jongh, M. Bulut, S. Donk, R. Kenmogne, A. Finiels, V. Hulea, F. Fajula, Zeolite Y crystals with trimodal porosity as ideal hydrocracking catalysts, Angew. Chem. Int. Ed., 49 (2010) 10074–10078.
[30] L. Li, P.A. Quinlivan, D.R.U. Knappe, Effects of activated carbon surface chemistry and pore structure on the adsorption of organic contaminants from aqueous solution, Carbon, 40 (2002) 2085–2100.
[31] A. Gil, F.C.C. Assis, S. Albeniz, S.A. Korili, Removal of dyes from wastewaters by adsorption on pillared clays, Chem. Eng. J., 168 (2011) 1032–1040.
[32] T. Hua, R. Haynes, Y.-F. Zhou, A. Boullemant, I. Chandrawana, Potential for use of industrial waste materials as filter media for removal of Al, Mo As, V and Ga from alkaline drainage in constructed wetlands-adsorption studies, Water Res., 71 (2015) 32–42.
[33] Y.-S. Ho, G. McKay, Pseudo-second order model for sorption processes, Process Biochem., 34 (1999) 451–465.
[34] F. Lyu, S. Niu, L. Wang, R. Liu, W. Sun, D. He, Efficient removal of Pb(II) ions from aqueous solution by modified red mud, J. Hazard. Mater., 406 (2021) 124678, doi: 10.1016/j.jhazmat.2020.124678.
[35] C. Shi, F. Tao, Y. Cui, Evaluation of nitriloacetic acid modified cellulose film on adsorption of methylene blue, Int. J. Biol. Macromol., 114 (2018) 400–407.
[36] P. Wu, Q. Zhang, Y. Dai, N. Zhu, Z. Dang, P. Li, J. Wu, X. Wang, Adsorption of Cu(II), Cd(II) and Cr(III) ions from aqueous solutions on humic acid modified Ca-montmorillonite, Geoderma, 164 (2011) 215–219.
[37] M. Dogan, M. Alkan, Adsorption kinetics of methyl violet onto perlite, Chemosphere, 50 (2003) 517–528.
[38] B. Gu, J. Schmitt, Z. Chen, L. Liang, J.F. McCarthy, Adsorption and desorption of natural organic matter on iron oxide: mechanisms and models, Environ. Sci. Technol., 28 (1994) 38–46.
[39] Q. Li, Q.-Y. Yue, Y. Su, B.-Y. Gao, H.-J. Sun, Equilibrium, thermodynamics and process design to minimize adsorbent amount for the adsorption of acid dyes onto cationic polymer-loaded bentonite, Chem. Eng. J., 158 (2010) 489–497.
[40] F.-C. Wu, R.-L. Tseng, R.-S. Juang, Characteristics of elovich equation used for the analysis of adsorption kinetics in dye-chitosan systems, Chem. Eng. J., 150 (2009) 366–373.
[41] R.R. Pawar, Lalhmunsiama, P. Gupta, S.Y. Sawant, B. Shahmoradi, S.-M. Lee, Porous synthetic hectorite clay-alginate composite beads for effective adsorption of methylene blue dye from aqueous solution, Int. J. Biol. Macromol., 114 (2018) 1315–1324.
[42] S. Mnasri, N. Hamdi, N. Frini-Srasra, E. Srasra, Acid-base properties of pillared interlayered clays with single and mixed Zr-Al oxide pillars prepared from tunisian-interstratified illite-smectite, Arabian J. Chem., 10 (2017) 1175–1183.
[43] W.H. Li, Q.Y. Yue, B.Y. Gao, Z.H. Ma, Y.J. Li, H.X. Zhao, Preparation and utilization of sludge-based activated carbon for the adsorption of dyes from aqueous solutions, Chem. Eng. J., 171 (2011) 320–327.
[44] Z. Heidarinejad, O. Rahmanian, M. Fazlzadeh, M. Heidari, Enhancement of methylene blue adsorption onto activated carbon prepared from date press cake by low frequency ultrasound, J. Mol. Liq., 264 (2018) 591–599.